ISSN 1674-1056
http://cpb.iphy.ac.cn
http://iopscience.iop.org/cpb
中国物理 B
Chinese Physics
中国物理 Chinese Physics B

## Dependence of photoelectron-momentum distribution of $H_2^+$ molecule on orientation angle and laser ellipticity

Hong-Dan Zhang(张宏丹), Si-Qi Zhang(张思琪), Lei Ji(纪磊), Qi Zhen(甄琪), Jing Guo(郭静), Xue-Shen Liu(刘学深)

**Citation:**Chin. Phys. B . 2019, 28(5): 053201. **doi:** 10.1088/1674-1056/28/5/053201
Journal homepage: http://cpb.iphy.ac.cn; http://iopscience.iop.org/cpb

**What follows is a list of articles you may be interested in**

---

## Femtosecond strong-field coherent control of nonresonant ionization with shaped pulses

Qiu-Nan Tong(佟秋男), Zhen-Zhong Lian(廉振中), Liang Zhao(赵亮), Hong-Xia Qi(齐洪霞), Zhou Chen(陈洲), Zhan Hu(胡湛)

Chin. Phys. B . 2019, 28(3): 033201. **doi:** 10.1088/1674-1056/28/3/033201

## Angle-resolved spectra of the direct above-threshold ionization of diatomic molecule in IR+XUV laser fields

Shang Shi(石尚), Fa-Cheng Jin(金发成), Bing-Bing Wang(王兵兵)

Chin. Phys. B . 2019, 28(2): 023202. **doi:** 10.1088/1674-1056/28/2/023202

## Validity of extracting photoionization time delay from the first moment of streaking spectrogram

Chang-Li Wei(魏长立), Xi Zhao(赵曦)

Chin. Phys. B . 2019, 28(1): 013201. **doi:** 10.1088/1674-1056/28/1/013201

## Low-order harmonic generation of hydrogen molecular ion in laser field studied by the two-state model

Ling-Ling Du(杜玲玲), Guo-Li Wang(王国利), Peng-Cheng Li(李鹏程), Xiao-Xin Zhou(周效信)

Chin. Phys. B . 2018, 27(11): 113201. **doi:** 10.1088/1674-1056/27/11/113201

## Interpulse interference of electron emission from an atom irradiated by sinusoidally phase-modulated pulse

Hai-Ying Yuan(袁海颖), Fu-Ming Guo(郭福明), Di-Yu Zhang(张頔玉), Jun Wang(王俊), Ji-Gen Chen(陈基根), Yu-Jun Yang(杨玉军)

Chin. Phys. B . 2018, 27(10): 103201. **doi:** 10.1088/1674-1056/27/10/103201

---

# Dependence of photoelectron-momentum distribution of $H_2^+$ molecule on orientation angle and laser ellipticity*

Hong-Dan Zhang(张宏丹)[1], Si-Qi Zhang(张思琪)[1], Lei Ji(纪磊)[2], Qi Zhen(甄琪)[1], Jing Guo(郭静)[1,†], and Xue-Shen Liu(刘学深)[1,‡]

[1] *Institute of Atomic and Molecular Physics, Jilin University, Changchun* 130012, *China*
[2] *School of Physics and Electronic Technology, Liaoning Normal University, Dalian* 116029, *China*

(Received 15 February 2019; revised manuscript received 7 March 2019; published online 22 April 2019)

By numerically solving the two-dimensional time-dependent Schrödinger equation under the frozen-nuclei approximation, we are able to study the molecular photoelectron-momentum distribution (MPMD) of $H_2^+$ with different orientation angles driven by elliptically polarized laser pulse with varying ellipticities. Our numerical results show that the MPMD is sensitive to the orientation angle and the laser ellipticity, which can be explained by the attosecond perturbation ionization theory and the exactly solvable photoionization model. When the ellipticity $\varepsilon = 0$, the final MPMD of $x$-oriented $H_2^+$ shows a distinct six-lobe pattern that is different from that with $\varepsilon = 0.5$ and $\varepsilon = 1$. The evolutions of electron wave packet (EWP) and MPMD with $x$-oriented $H_2^+$ are presented to interpret this distinct pattern.

**Keywords:** $H_2^+$ molecule, molecular photoelectron-momentum distribution, attosecond perturbation ionization theory

**PACS:** 32.80.Rm, 32.80.Fb, 42.65.Re **DOI:** 10.1088/1674-1056/28/5/053201

## 1. Introduction

The rapid development of ultrashort laser pulses offers the possibility for investigating electron dynamics on its natural attosecond (1 as = $10^{-18}$ s) time scale.[1–5] Attosecond pulses allow us to separate electronic (attosecond time scale) and nuclear (femtosecond time scale, 1 fs = $10^{-15}$ s) effects. Thus, one can study electronic dynamics regardless of the interference from nuclear motion. The attosecond pulse can be obtained by superposing some orders from high harmonic generation.[6,7] To date, the shortest single attosecond soft-x-ray pulse of 43 as has been obtained by Gaumnitz *et al.*[8] One can thus watch pure electronic quantum effects through attosecond imaging.[9]

Ultraviolet (UV) laser pulses have been used as a powerful and efficient tool for the research on electron dynamics. The attosecond extreme ultraviolet (XUV) transient absorption spectroscopy has been widely applied to many ultrafast dynamical processes, including the measurement of valence electrons,[3] the study of autoionization of atoms,[10] and probing the time-dependent molecular dipoles.[11] It has also been employed as a probing pulse in the real-time probing of the electron dynamics of an atom. XUV probing can also be applied to explore the excitation dynamics during and after the infrared (IR) pump pulse interaction.[12]

The research on the simplest $H_2^+$ molecule providing an ideal prototype for diatomic molecules has attracted much attention, and it has been served as a vehicle to understand and explore some basic physical processes such as high harmonic generation,[13–16] the double-slit interference effect,[17,18] the dissociation of $H_2^+$ molecule,[19,20] and the photoionization[21–23] and photoelectron-momentum distribution (PMD).[24–26]

The strong field electron emission from $H_2^+$ has been studied experimentally. Odenweller *et al.*[27] found that the observed unexpected time instants and initial velocities for the electron emission are due to a complex electronic motion inside $H_2^+$. The molecular photoelectron-momentum distribution (MPMD) by bichromatic circularly polarized attosecond UV laser pulse has been theoretically studied, and the MPMDs exhibit a spiral structure for both co-rotating and counter-rotating schemes.[28] We researched the sensitivity of MPMD and molecular photoelectron angular distribution (MPAD) of $H_2^+$ to internuclear distance, laser ellipticity, as well as the wavelength. In addition, laser-induced electron diffraction (LIED)[21] occurred when the wavelength is changed from 35 nm to 5 nm.[29] Guan *et al.*[30] theoretically investigated the multiphoton ionization of $H_2^+$ irradiated by ultrashort elliptically polarized laser pulse for changing central photon energies and they found that the confinement effect observed in linearly polarized laser pulse still exists in elliptically polarized laser pulse. The effect of Coulomb potential on MPMD has been investigated by screening the Coulomb potential at

*Project supported by the National Natural Science Foundation of China (Grant Nos. 11271158, 11574117, and 61575077) and the Natural Science Foundation of Jilin Province of China (Grants No. 20180101225JC).

†Corresponding author. E-mail: gjing@jlu.edu.cn
‡Corresponding author. E-mail: liuxs@jlu.edu.cn

© 2019 Chinese Physical Society and IOP Publishing Ltd 

different radii based on classical trajectory calculations and it presents a picture of how the trajectories are bent by the Coulomb potential.[31] The research on MPMD is not constrained within $H_2^+$. Some studies aimed at molecular orbital imaging via MPMD of $N_2$, $CO_2$, and so on.[32]

In this paper, we investigate the MPMD of $H_2^+$ under elliptically polarized laser pulse. The MPMDs exhibit different patterns under varying orientation angles and laser ellipticities. We use the attosecond perturbation ionization theory and the exactly solvable photoionization model to quantitatively interpret the variation of MPMDs along with different orientation angles and laser ellipticities. The evolutions of electron wave packet (EWP) and MPMD are also presented to further explain the distinct pattern of MPMD for the ellipticity $\varepsilon = 0$ when $H_2^+$ is fixed along the $x$-axis.

## 2. Theoretical model

We consider a fixed nuclei $H_2^+$ with different orientations exposed to the elliptically polarized laser pulse with varying ellipticities. The two-dimensional (2D) time-dependent Schrödinger equation (TDSE) under the frozen-nuclei approximation is

$$\mathrm{i}\frac{\partial \phi(x,y,t)}{\partial t} = \left[\frac{p_x^2+p_y^2}{2} + V(x,y) + xE_x(t) + yE_y(t)\right]\phi(x,y,t). \quad (1)$$

The atomic units (a.u.) are used throughout unless stated otherwise. The soft-core Coulomb potential can be expressed as

$$V(x,y) = -\frac{1}{\sqrt{(x-\frac{R_e}{2}\cos\theta)^2+(y-\frac{R_e}{2}\sin\theta)^2+c}} - \frac{1}{\sqrt{(x+\frac{R_e}{2}\cos\theta)^2+(y+\frac{R_e}{2}\sin\theta)^2+c}}, \quad (2)$$

where $R_e = 2$ a.u. is the equilibrium internuclear distance, $c = 0.5$ is the soft-core parameter which is chosen to obtain the ionization potential of $H_2^+$ molecule, $\theta$ is the orientation angle between the molecular axis and the $x$-axis, $E_x(t)$ and $E_y(t)$ are the $x$ and $y$ components of the laser field, and $p_x$ and $p_y$ are the momentum operators in the $x$- and $y$-direction.

This research is based on solving 2D TDSE by the splitting-operator fast-Fourier transform algorithm.[33] The initial wave packet can be constructed by propagating an initial appropriate wavefunction in imaginary time. The spatial coordinates are discretized by the grid points extending from $-204.8$ a.u. to 204.8 a.u. containing 1024 grid points in both $x$- and $y$-directions. During the calculation, the wave packets are multiplied by a $\cos^{1/8}$ mask function in each step to suppress the non-physical reflection at the boundaries. The absorber domain in both $x$- and $y$-directions range from 150 a.u. to 204.8 a.u. At the final propagation time, the wave packet is multiplied by a mask function $M(r)$ that splits the wave packet into ionized part and bounded part.[34] The MPMD can be obtained by Fourier transforming the ionized wave packet. Another four optical cycles are propagated after the end of the laser pulse to collect the "slow" photoelectrons. The MPMDs are converged with respect to the final time.

## 3. Results and discussion

The elliptically polarized laser field in our simulation is

$$\boldsymbol{E}(t) = E_0 f(t)\left[\frac{1}{\sqrt{1+\varepsilon^2}}\cos(\omega t)\hat{e}_x + \frac{\varepsilon}{\sqrt{1+\varepsilon^2}}\sin(\omega t)\hat{e}_y\right], \quad (3)$$

where $\omega = 1.52$ a.u. ($\lambda = 30$ nm) is the laser angular frequency, $E_0 = 0.12$ a.u. ($I_0 = 5\times10^{14}$ W/cm$^2$) is the maximum field strength of the laser field, $\varepsilon$ is the ellipticity of the laser field, and $f(t) = \sin(\pi t/nT)^2$ is the laser envelope; the pulse lasts for 10 optical cycles ($n = 10$). In our calculation, the single-photon process is considered which means that the electron can be ionized by absorbing only one photon ($\omega > I_p = 1.1$ a.u.).

Figure 1 shows the molecular Coulomb potential and MPMD with different orientation angles and laser ellipticities. It can be seen from Figs. 1(d)–1(f) and Figs. 1(g)–1(i) that the MPMDs with $\varepsilon = 0.5$ and $\varepsilon = 1.0$ are all localized mainly in two parts, and the distributions are all perpendicular to the molecular axis with relative small tilted angles which come from the effect of Coulomb potential and the helicity of the laser field.[27,35] Our previous theoretical research (calculated by 30 nm laser pulse)[29] has shown similar distribution pattern with that under the experimental result (by 800 nm laser pulse).[27] The classical analysis has also verified the effect of Coulomb potential on the distortion of MPMD, and the research shows that the tilted angle would increase as the laser intensity increases.[36]

The orientation effect on MPMD has previously been studied.[37] These authors researched the orientation of $H_2^+$ molecule relative to the plane of laser polarization within three-dimensional system by the 800 nm few-cycle high-intensity near-infrared circularly polarized laser field and their results showed a significant impact of orientation on the PMDs due to the anisotropic molecular potential and the orientation-dependent coupling between the ground state and excited states. In our calculations, we choose the 30 nm attosecond UV laser field with varying ellipticity to study the orientation dependence of $H_2^+$ molecule in the laser polarization plane within 2D system.

Our results can be explained well by the attosecond perturbation ionization theory[38,39] and the exactly solvable photoionization model of $H_2^+$ using the $\delta$-function pulse.[21,23,29]

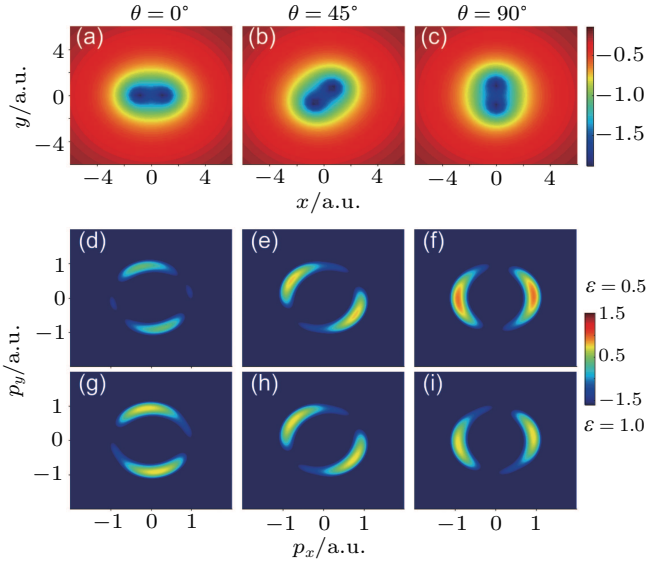



**Fig. 1.** Coulomb potential of $H_2^+$ with different orientation angles $\theta$ and MPMD of $H_2^+$ with different $\theta$ and ellipticities $\varepsilon$. The first column, i.e., (a), (d), and (g), is for the case of $\theta = 0°$; the second column, i.e., (b), (e), and (h), is for the case of $\theta = 45°$; the third column, i.e., (c), (f), and (i), is for the case of $\theta = 90°$. The first row (a)–(c) is the Coulomb potential with three orientation angles, and the intensities are on a linear scale; the second row (d)–(f) is the MPMD with $\varepsilon = 0.5$ (elliptically polarized laser field), and the third row (g)–(i) is the MPMD with $\varepsilon = 1.0$ (circularly polarized laser field), the intensities are on a logarithmic scale.

The single ionization amplitude can be written as

$$A^{(x)} = \langle \phi_c | \boldsymbol{r} \cdot \boldsymbol{E}_x | \phi_0 \rangle = \sigma^{(x)} E_x(k) \cos(\alpha), \tag{4}$$

$$A^{(y)} = \langle \phi_c | \boldsymbol{r} \cdot \boldsymbol{E}_y | \phi_0 \rangle = \sigma^{(y)} E_y(k) \sin(\alpha), \tag{5}$$

where $\sigma^{(x)} = \langle \phi_c | x | \phi_0 \rangle$ and $\sigma^{(y)} = \langle \phi_c | y | \phi_0 \rangle$ are the transition matrix elements along the $x$ and $y$ directions, $\alpha$ is the angle between the photoelectron momentum $\boldsymbol{p}$ and the $x$-axis, $|\phi_0\rangle$ and $|\phi_c\rangle$ are the initial ground state and continuum state, respectively, and $E_x(k) = E_{x_0}(k)\dfrac{1}{\sqrt{1+\varepsilon^2}}$ and $E_y(k) = E_{y_0}(k)\dfrac{\varepsilon}{\sqrt{1+\varepsilon^2}}$ are the pulse frequency shape as a Fourier transform of the pulse along the $x$ and $y$ directions, where $E_{x_0}(k) = \int_{-\infty}^{\infty} E_0 f(t) \cos(\omega t) e^{ikt} dt$ and $E_{y_0}(k) = \int_{-\infty}^{\infty} E_0 f(t) \sin(\omega t) e^{ikt} dt$. The total distribution reads

$$|A|^2 = |A^{(x)}|^2 + |A^{(y)}|^2 + A^{(x,y)}, \tag{6}$$

where the interference term is

$$\begin{aligned} A^{(x,y)} &= A^{(x)*} A^{(y)} + A^{(x)} A^{(y)*} \\ &= \sigma^{(x)} \sigma^{(y)} E_x(k) E_y(k) \sin(2\alpha). \end{aligned} \tag{7}$$

For $H_2^+$ with two centers, the corresponding MPMD is the superposition of ionization from the two nuclei. According to the exactly solvable photoionization model of $H_2^+$ by $\delta$-function pulse which has described LIED in ultrafast laser fields before,[21] the wavefunction in momentum space right after the pulse is

$$\psi(\boldsymbol{p}, 0^+) = \psi(\boldsymbol{p} + \boldsymbol{F}), \tag{8}$$

where $\boldsymbol{p}$ and $\boldsymbol{F}$ represent the momentum vector of electron and field vector, respectively. The wavefunction in the coordinate space can be obtained by Fourier transforming the wavefunction in the momentum space, which is

$$\begin{aligned} \psi(\boldsymbol{r}, 0^+) &= (2\pi)^{-\frac{3}{2}} \int e^{-i\boldsymbol{p}\cdot\boldsymbol{r}} \psi(\boldsymbol{p}, 0^+) d\boldsymbol{p} \\ &= e^{-i\boldsymbol{F}\cdot\boldsymbol{r}} \psi_0(\boldsymbol{r}), \end{aligned} \tag{9}$$

where $\psi_0(\boldsymbol{r})$ is the initial wavefunction in the coordinate space. Then, the transition amplitude can be written as[40]

$$\begin{aligned} A(\boldsymbol{p}) &\propto (2\pi)^{-\frac{3}{2}} \int e^{-i\boldsymbol{p}\cdot\boldsymbol{r}} \psi(\boldsymbol{r}, 0^+) d\boldsymbol{r} \\ &= (2\pi)^{-\frac{3}{2}} \int e^{-i\boldsymbol{p}\cdot\boldsymbol{r}} e^{-i\boldsymbol{F}\cdot\boldsymbol{r}} \psi_0(\boldsymbol{r}) d\boldsymbol{r}. \end{aligned} \tag{10}$$

The wave function of the 1s atomic orbital of $H_2^+$ is $\psi_{1s\sigma_g} = \psi_{1s}(\boldsymbol{r} - \boldsymbol{R}/2) + \psi_{1s}(\boldsymbol{r} + \boldsymbol{R}/2)$, which is the linear combinations of hydrogenic 1s orbital located at $\pm R/2$. By taking attosecond perturbation ionization theory into account, the transition amplitude can thus be rewritten as

$$\begin{aligned} A^{(x)}_{\sigma_g} &\propto \sqrt{2} c^{(x)} E_{x_0}(k) \frac{1}{\sqrt{1+\varepsilon^2}} \cos(\alpha) \\ &\quad \times \cos[(\boldsymbol{p} + \boldsymbol{F}) \cdot \boldsymbol{R}/2] \psi_{1s}(|\boldsymbol{p} + \boldsymbol{F}|), \end{aligned} \tag{11}$$

$$\begin{aligned} A^{(y)}_{\sigma_g} &\propto \sqrt{2} c^{(y)} E_{y_0}(k) \frac{\varepsilon}{\sqrt{1+\varepsilon^2}} \sin(\alpha) \\ &\quad \times \cos[(\boldsymbol{p} + \boldsymbol{F}) \cdot \boldsymbol{R}/2] \psi_{1s}(|\boldsymbol{p} + \boldsymbol{F}|). \end{aligned} \tag{12}$$

Here, $|c^{(x)}|^2$ and $|c^{(y)}|^2$ are the ionization probabilities along the $x$ and $y$ directions, respectively. Note that in the current calculations, the pulse field $\boldsymbol{F}$ can be ignored since the ponderomotive energies $U_p \ll I_p$ and $F \ll p$ in chosen intensity, which is

$$A^{(x)}_{\sigma_g} \propto \sqrt{2} c^{(x)} E_{x_0}(k) \frac{1}{\sqrt{1+\varepsilon^2}} \cos(\alpha) \cos(\boldsymbol{p} \cdot \boldsymbol{R}/2) \psi_{1s}(|\boldsymbol{p}|), \tag{13}$$

$$A^{(y)}_{\sigma_g} \propto \sqrt{2} c^{(y)} E_{y_0}(k) \frac{\varepsilon}{\sqrt{1+\varepsilon^2}} \sin(\alpha) \cos(\boldsymbol{p} \cdot \boldsymbol{R}/2) \psi_{1s}(|\boldsymbol{p}|). \tag{14}$$

Thus, the interference term can be expressed as

$$\begin{aligned} A^{(x,y)}_{\sigma_g} &= A^{(x)*} A^{(y)} + A^{(x)} A^{(y)*} \\ &\propto 2 c^{(x)} c^{(y)} E_x(k) E_y(k) \sin(2\alpha) \\ &\quad \times \cos^2(\boldsymbol{p} \cdot \boldsymbol{R}/2) \psi^2_{1s}(|\boldsymbol{p}|). \end{aligned} \tag{15}$$

The maximum distribution meets $\cos^2(\boldsymbol{p} \cdot \boldsymbol{R}/2) = \cos^2(pR\cos\theta_{pR}/2) = 1$, then $\theta_{pR} = n\pi + \pi/2$, $n = 0, \pm 1, \pm 2, \ldots$, with $\theta_{pR}$ being the angle between the photoelectron momentum $\boldsymbol{p}$ and the molecular axis, which means that the maximum distribution always lies in the perpendicular direction to the molecular axis which gives a good theoretical explanation. We have also tested the larger orientation angles up to 180°, and the tendency keeps the same as that in Fig. 1. Besides, we have also considered the MPMD under different orientation angles and internuclear distances; the distribution

under different conditions shows the same characteristic that is perpendicular to the molecular axis, which is not shown here.

Note that for the orientation angle $\theta = 0°$, the intensity of MPMD under $\varepsilon = 1.0$ (circularly polarized laser field) case (Fig. 1(g)) is more intense than that under $\varepsilon = 0.5$ (elliptically polarized laser field) case (Fig. 1(d)). And when $\theta = 90°$, the results reverse.

For $\theta = 0°$, the maximum distribution mainly lies in the $y$ direction with a small tilted angle; we focus on the module square of transition amplitude along the $y$ direction

$$|A_{\sigma_g}^{(y)}|^2 \propto 2|c^{(y)}|^2 E_{y_0}^2(k)\frac{\varepsilon^2}{1+\varepsilon^2}\sin^2(\alpha) \times \cos^2(\boldsymbol{p}\cdot\boldsymbol{R}/2)\psi_{1s}^2(|\boldsymbol{p}|). \quad (16)$$

The values for $\varepsilon^2/(1+\varepsilon^2)$ are 0.2 and 0.5 when $\varepsilon = 0.5$ and $\varepsilon = 1.0$, respectively, which explains the more intense distribution in Fig. 1(g) than that in Fig. 1(d).

Similarly, for $\theta = 90°$, the maximum distribution mainly lies in the $x$ direction, and the module square of transition amplitude along the $x$ direction reads

$$|A_{\sigma_g}^{(x)}|^2 \propto 2|c^{(x)}|^2 E_{x_0}^2(k)\frac{1}{1+\varepsilon^2}\cos^2(\alpha) \times \cos^2(\boldsymbol{p}\cdot\boldsymbol{R}/2)\psi_{1s}^2(|\boldsymbol{p}|). \quad (17)$$

When $\varepsilon = 0.5$ and $\varepsilon = 1.0$, $1/(1+\varepsilon^2)$ values are respectively 0.8 and 0.5; thus, we have an intuitive description for the more intense distribution in Fig. 1(f) than that in Fig. 1(i).

Figure 2 shows the MPMD of $H_2^+$ with different orientation angles under linearly polarized laser field ($\varepsilon = 0$). For linearly polarized laser field, the transition amplitude can be written as

$$A_{\sigma_g} \propto (2\pi)^{-\frac{3}{2}}\sqrt{2}\cos(\boldsymbol{p}\cdot\boldsymbol{R}/2)\psi_{1s}(|\boldsymbol{p}|). \quad (18)$$

The maximum distribution still lies in the direction perpendicular to the molecular axis as stated above. However, for orientation angle $\theta = 0°$, the MPMD shows a distinct pattern with six lobes as demonstrated in Fig. 2(a).

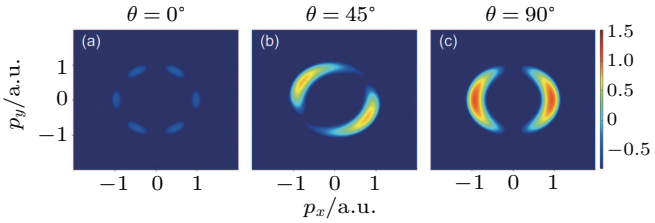



**Fig. 2.** The 2D MPMD of $H_2^+$ under linearly polarized laser field with orientation angle (a) $\theta = 0°$, (b) $\theta = 45°$, and (c) $\theta = 90°$; the intensities are on a logarithmic scale.

To further understand the mechanism of the distinct MPMD of $x$-oriented $H_2^+$ ($\theta = 0$), the evolutions of the EWP and MPMD under linearly polarized laser field ($\varepsilon = 0$) and under an elliptically polarized laser field ($\varepsilon = 0.5$) are shown in Figs. 3 and 4, respectively.

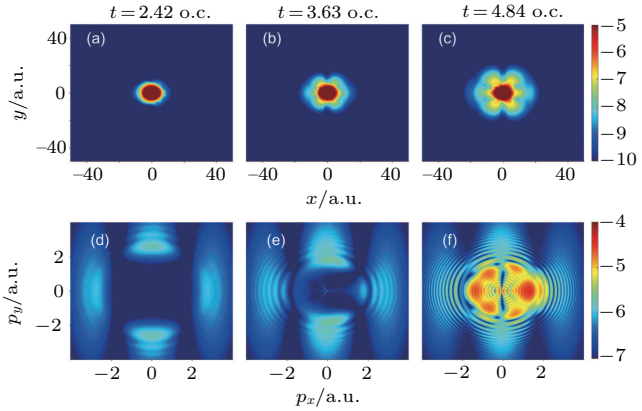



**Fig. 3.** The 2D EWP and MPMD of $x$-oriented $H_2^+$ ($\theta = 0$) under linearly polarized laser field ($\varepsilon = 0$) at: (a) and (d) $t = 2.42$ o.c.; (b) and (e) $t = 3.63$ o.c.; (c) and (f) $t = 4.84$ o.c. Here, o.c. denotes the optical cycle; the intensities are on a logarithmic scale.

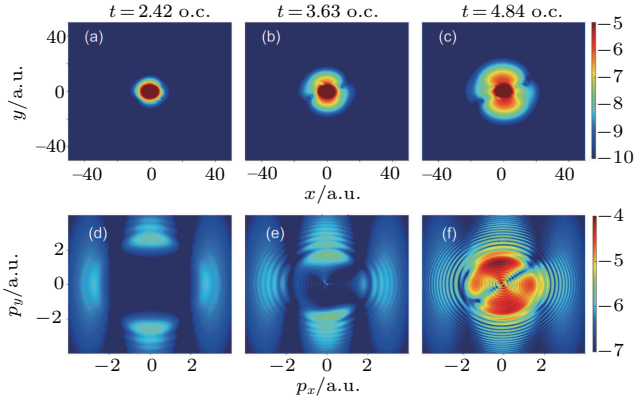



**Fig. 4.** The 2D EWP and MPMD of $x$-oriented $H_2^+$ ($\theta = 0$) under an elliptically polarized laser field ($\varepsilon = 0.5$) at: (a) and (d) $t = 2.42$ o.c.; (b) and (e) $t = 3.63$ o.c.; (c) and (f) $t = 4.84$ o.c.; the intensities are on a logarithmic scale.

The evolutions of EWP in Figs. 3(a)–3(c) show the movement of photoelectron under linearly polarized laser field ($\varepsilon = 0$). At $t = 2.42$ optical cycle (o.c.), the electron is not ionized yet, and the electron is mainly localized around the molecular nuclei; at $t = 3.63$ o.c., the electron has been ionized in six directions; at $t = 4.84$ o.c., the EWP has evolved further in six directions.

The evolution of MPMD makes the process of photoelectron movement much clear. In Fig. 3(d), the MPMD is mainly localized in the region where the initial MPMD lies because the electron is not ionized yet. At $t = 3.63$ o.c. (Fig. 3(e)), the distribution starts to present an interference pattern as "multi-ring" structure, which originates from the coherent superposition from EWPs ionized at different times with the same momentum. In Fig. 3(f), the MPMD at $t = 4.84$ o.c. presents six lobes which is similar to the final MPMD and more interference stripes, and the "multi-ring" structure becomes much narrower. As time evolves from $t = 2.42$ o.c. to $t = 4.84$ o.c.,

more electrons are ionized and involved in the coherent superposition, resulting in the appearance of more interference stripes.

The evolutions of EWP and MPMD under an elliptically polarized laser field ($\varepsilon = 0.5$) at the same time are shown in Fig. 4 for clear comparison. The EWP at $t = 2.42$ o.c. in Fig. 4(a) has the similar distribution as that in Fig. 3(a) which is not ionized yet. At $t = 3.63$ o.c., the EWP in Fig. 4(b) shows that the electron starts to ionize mainly along the $y$ direction. In Fig. 4(c), at $t = 4.84$ o.c., the EWP evolves along the $y$ direction much further.

The MPMDs at $t = 2.42$ o.c. (Fig. 4(d)) and $t = 3.63$ o.c. (Fig. 4(e)) under an elliptically polarized laser field present similar distribution as that in Figs. 3(d) and 3(e) under linearly polarized laser field. However, the MPMD at $t = 4.84$ o.c. presents the main distribution along the $y$ direction which has presented the appearance of final MPMD as shown in Fig. 1(d). Besides, the MPMD in Fig. 4(f) also shows fruitful interference stripes similar to that in Fig. 3(f), which is due to the coherent superposition of EWP ionized at different times with the same momentum. Thus, it can be seen from Figs. 3 and 4 that the final MPMD can be influenced by the ellipticity of the laser field.

## 4. Conclusions

In summary, we study the MPMD of $H_2^+$ with different orientation angles in an elliptically polarized laser field by numerically solving the 2D TDSE under the frozen-nuclei approximation. Our numerical results show the dependence of MPMD on orientation angle and laser ellipticity. The attosecond perturbation ionization theory and the exactly solvable photoionization model are employed to explain the results. The evolutions of both EWP and MPMD with $\theta = 0^\circ$ under linearly and elliptically polarized laser pulses are presented to interpret the distinct final MPMD pattern with $\theta = 0^\circ$ under linearly polarized laser pulse.

## References


[1] Hentschel M, Kienberger R, Spielmann Ch, Reider G A, Milosevic N, Corkum P B, Heinzmann U, Drescher M and Krausz F 2001 *Nature* **414** 509

[2] Krausz F and Ivanov M 2009 *Rev. Mod. Phys.* **81** 163

[3] Goulielmakis E, Loh Z H, Wirth A, Santra R, Rohringer N, Yakovlev V S, Zherebtsov S, Pfeifer T, Azzeer A M, Kling M F, Leone S R and Krausz F 2010 *Nature* **466** 739

[4] Haessler S, Caillat J, Giovanetti-Teixeira C, Ruchon T, Auguste T, Diveki Z, Breger P, Maquet A, Carr'e B, Taïeb R and Salières P 2010 *Nat. Phys.* **6** 200

[5] Xiao X R, Wang M X, Li M, Geng J W, Liu Y Q and Peng L Y 2016 *Acta Phys. Sin.* **65** 220203 (in Chinese)

[6] Jia Y W, Guo Q L, Li P C, Wang G L and Zhou X X 2016 *Acta Phys. Sin.* **65** 223205 (in Chinese)

[7] Zhang H D, Guo J, Shi Y, Du H, Liu H F, Huang X R, Liu X S and Jing J 2017 *Chin. Phys. Lett.* **34** 014206

[8] Gaumnitz T, Jain A, Pertot Y, Huppert M, Jordan I, Ardana-Lamas F and Wörner H J 2017 *Opt. Express* **25** 27506

[9] Vrakking M J J 2014 *Phys. Chem. Chem. Phys.* **16** 2775

[10] Wang H, Chini M, Chen S, Zhang C, He F, Cheng Y, Wu Y, Thumm U and Chang Z 2010 *Phys. Rev. Lett.* **105** 143002

[11] Neidel Ch, Klei J, Yang C H, Rouzée A, Vrakking M J J, Klünder K, Miranda M, Arnold C L, Fordell T, L'Huillier A, Gisselbrecht M, Johnsson P, Dinh M P, Suraud E, Reinhard P G, Despré V, Marques M A L and Lépine F 2013 *Phys. Rev. Lett.* **111** 033001

[12] Deng Y P and Xie X H 2015 *Phys. Rev. A* **91** 043414

[13] Zhang J, Ge X L, Wang T, Xu T T, Guo J and Liu X S 2015 *Phys. Rev. A* **92** 013418

[14] Pan X F, Zhang J, Luo X Y, Zhang H D, Xu T T and Liu X S 2018 *Laser Phys.* **28** 075301

[15] Yuan K J and Bandrauk A D 2018 *Phys. Rev. A* **97** 023408

[16] Miller M R, Jaroń-Becker A and Becker A 2016 *Phys. Rev. A* **93** 013406

[17] Picón A, Bahabad A, Kapteyn H C, Murnane M M and Becker A 2011 *Phys. Rev. A* **83** 013414

[18] Yuan K J, Bian X B and Bandrauk A D 2014 *Phys. Rev. A* **90** 023407

[19] Xu T Y and He F 2014 *Phys. Rev. A* **90** 053401

[20] Jiang S C, Yu C, Yuan G L, Wu T and Lu R F 2017 *Sci. Rep.* **7** 42086

[21] Zuo T, Bandrauk A D and Corkum P B 1996 *Chem. Phys. Lett.* **259** 313

[22] Guan X X, DuToit R C and Bartschat K 2013 *Phys. Rev. A* **87** 053410

[23] Yuan K J, Chelkowski S and Bandrauk A D 2015 *Chem. Phys. Lett.* **638** 173

[24] Murakami M and Chu S I 2016 *Phys. Rev. A* **94** 043425

[25] Yuan K J and Bandrauk A D 2012 *Phys. Rev. A* **85** 013413

[26] Yuan K J and Bandrauk A D 2012 *J. Phys. B: At. Mol. Opt. Phys.* **45** 105601

[27] Odenweller M, Takemoto N, Vredenborg A, Cole K, Pahl K, Titze J, Schmidt L P H, Jahnke T, Dörner R and Becker A 2011 *Phys. Rev. Lett.* **107** 143004

[28] Yuan K J, Chelkowski S and Bandrauk A D 2016 *Phys. Rev. A* **93** 053425

[29] Zhang H D, Ben S, Xu T T, Song K L, Tian Y R, Xu Q Y, Zhang S Q, Guo J and Liu X S 2018 *Phys. Rev. A* **98** 013422

[30] Guan X, Secor E B, Bartschat K and Schneider B I 2011 *Phys. Rev. A* **84** 033420

[31] Qin B Y, Wang P J and He F 2015 *Chin. Phys. B* **24** 114208

[32] Zhu X S, Zhang Q B, Lan P F and Lu P X 2016 *Acta Phys. Sin.* **65** 224207 (in Chinese)

[33] Feit M D, Fleck J A Jr. and Steiger A 1982 *J. Comput. Phys.* **47** 412

[34] He P L, Takemoto N and He F 2015 *Phys. Rev. A* **91** 063413

[35] Yuan K J, Chelkowski S and Bandrauk A D 2014 *Chem. Phys. Lett.* **592** 334

[36] Doblhoff-Dier K, Dimitriou K I, Staudte A and Gräfe S 2013 *Phys. Rev. A* **88** 033411

[37] Abu-samha M and Madsen L B 2016 *Phys. Rev. A* **94** 023414

[38] Pronin E A, Starace A F, Frolov M V and Manakov N L 2009 *Phys. Rev. A* **80** 063403

[39] Pronin E A, Starace A F and Peng L Y 2011 *Phys. Rev. A* **84** 013417

[40] Yuan K J and Bandrauk A D 2015 *Struct. Dynam.* **2** 014101